Volume 7 | Number 9 | 7 March 2015 | Pages 3789–4260

Nanoscale

www.rsc.org/nanoscale

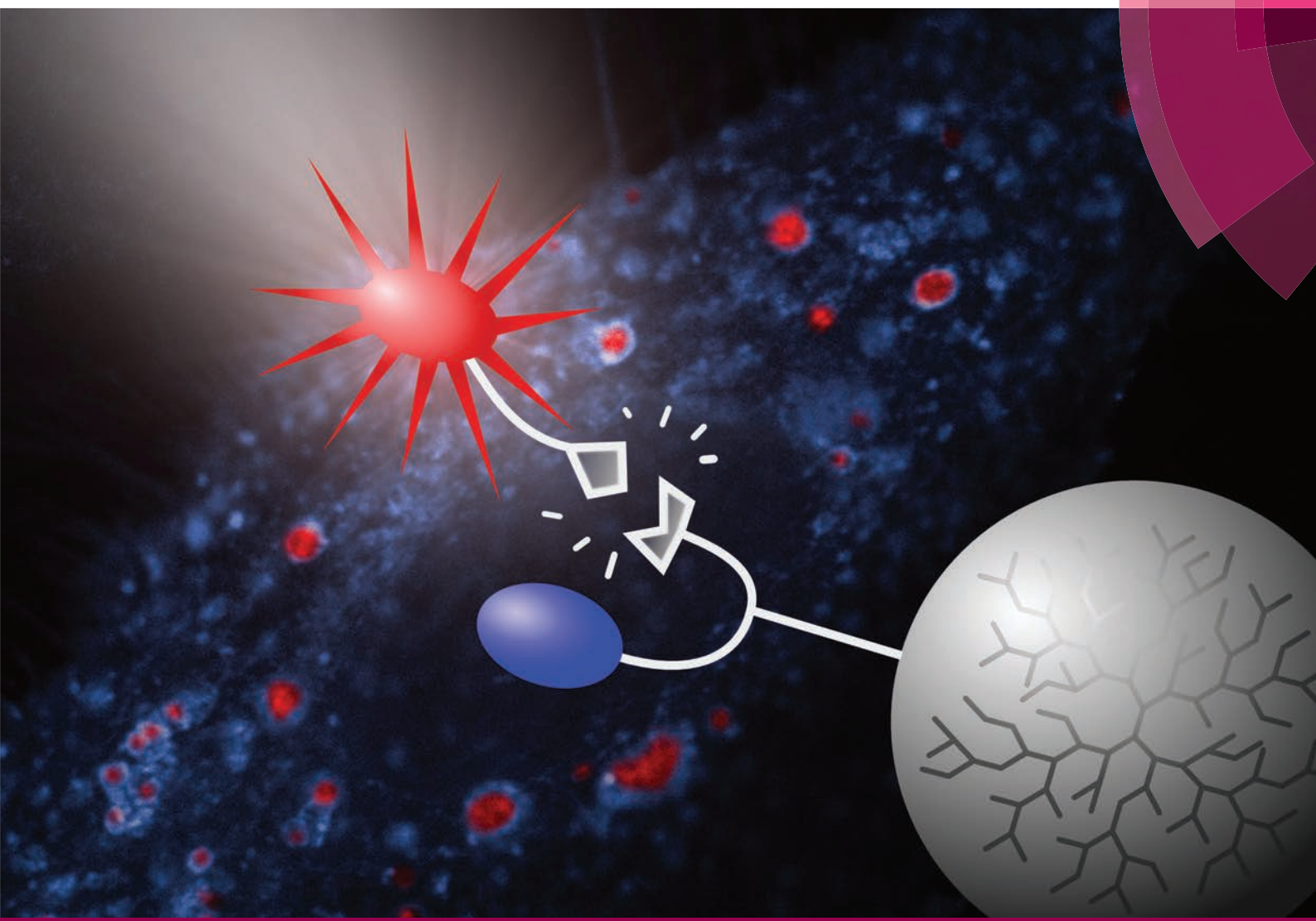

Themed issue: Dendritic polymers for smart drug delivery applications

ISSN 2040-3364

ROYAL SOCIETY OF CHEMISTRY

PAPER
Marcelo Calderón *et al.*
Dendritic polymer imaging systems for the evaluation of conjugate uptake and cleavage

NCNST

Nanoscale

PAPER

View Article Online
View Journal | View Issue

Cite this: *Nanoscale*, 2015, **7**, 3838

Dendritic polymer imaging systems for the evaluation of conjugate uptake and cleavage†

Harald R. Krüger, Gregor Nagel, Stefanie Wedepohl and Marcelo Calderón*

Received 4th August 2014,
Accepted 26th October 2014

DOI: 10.1039/c4nr04467c

www.rsc.org/nanoscale

Fluorescent turn-on probes combined with polymers have a broad range of applications, *e.g.* for intracellular sensing of ions, small molecules, or DNA. In the field of polymer therapeutics, these probes can be applied to extend the *in vitro* characterization of novel conjugates beyond cytotoxicity and cellular uptake studies. This is particularly true in cases in which polymer conjugates contain drugs attached by cleavable linkers. Better information on the intracellular linker cleavage and drug release would allow a faster evaluation and optimization of novel polymer therapeutic concepts. We therefore developed a fluorescent turn-on probe that enables direct monitoring of pH-mediated cleavage processes over time. This is achieved by exploiting the fluorescence resonance energy transfer (FRET) between two dyes that have been coupled to a dendritic polymer. We demonstrate the use of this probe to evaluate polymer uptake and intracellular release of cargo in a cell based microplate assay that is suitable for high throughput screening.

Introduction

The field of polymer therapeutics is evolving rapidly and thus producing a multitude of different drug delivery systems (DDS).[1] In general, these systems are composed of watersoluble polymers that act as inert functional nanocarriers to improve the delivery of drugs, imaging agents, proteins, or genes.[2] Polymer–drug conjugates can overcome the limitations of small molecule drugs due to a reduced body clearance, passive targeting, and controlled drug release all leading to a higher concentration of drugs at the site of action and minimized toxic side effects.[3]

After systemic application polymer–drug conjugates typically accumulate in solid tumors *via* the enhanced permeation and retention (EPR) effect.[4,5] They are taken up by cancer cells through endocytosis, which can be receptor mediated, adsorptive, or through the fluid-phase.[3] During endocytosis a significant drop in the pH value takes place from the physiological value (7.2–7.4) to 6.5–5.0 in the endosomes and to around 4.0 in the primary and secondary lysosomes. This drop in the pH was shown to be useful for triggering intracellular drug release from pH-sensitive nanocarriers.[3] Many acid cleavable bonds like hydrazones, acetals, and imines have been extensively explored as linkers between drugs and polymers.[6]

Imaging agents (fluorescent dyes, radionuclides, *etc.*) can be used in the same manner as drugs for conjugation to polymeric nanocarriers. Among the different imaging approaches, fluorescence resonance energy transfer (FRET) has been demonstrated to be a valuable tool for functional imaging in therapy and diagnosis.[7] The distance dependence makes FRET-based probes ideal for determining bond cleavage or changes in structural conformations of biomolecules.[8] FRET-based imaging is a powerful technique because it provides functional imaging with real time information and high sensitivity within intracellular milieu, *e.g.* monitoring of apoptosis,[9] enzyme activity,[10] or ion sensing.[11,12] Therefore, FRET-based applications may offer information on the release kinetics, which is crucial for the design of DDS.[7,13] In this regard versatile but complex nanoparticles which unite different imaging approaches and functional imaging through FRET have been reported.[14] They succeeded in providing detailed information achieved through *ad hoc* systems, *e.g.* studies of drug release through cleavage of crosslinked micelles,[15] release of a conjugated drug from a quantum dot or gold nanoparticles,[16] and release by diffusion of the encapsulated drug from mesoporous silica nanoparticles.[17] However, most of the reported systems are limited in terms of screening of multiple materials.

Gathering information about successful delivery and intracellular drug release of polymer–drug conjugates before expensive and time consuming *in vivo* investigations are performed, is of great importance. Cytotoxicity assays and

Institut für Chemie und Biochemie, Freie Universität Berlin, Takustrasse 3, 14195 Berlin, Germany. E-mail: marcelo.calderon@fu-berlin.de; http://www.bcp.fu-berlin.de; Fax: (+49) 30-838-459368

†Electronic supplementary information (ESI) available: Including detailed synthetic procedures of the dye and conjugate synthesis, as well as cellular uptake and inhibitor studies. See DOI: 10.1039/c4nr04467c

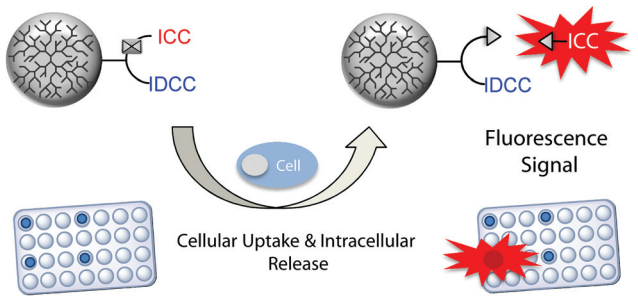

Scheme 1 Top: schematic illustration showing the mode of action of a FRET conjugate inducing a fluorescence signal upon uptake and release. Bottom: illustration of the plate reader assay related to the mode of action of the FRET conjugate.

fluorescence microscopy are nowadays the main tools for evaluating the performance of DDS *in vitro*. Although they provide valuable information, *e.g.* cytotoxicity and details about intracellular fate, these assays do not allow correlation of the performance of DDS with their cellular uptake and drug release.

Herein, we present a turn-on probe that overcomes the aforementioned limitation and enables the fast and simultaneous screening of DDS in a simple cell-based microplate assay. The probe comprises a fluorescent donor and an acceptor dye (indocarbocyanine [ICC] and indodicarbocyanine [IDCC], respectively) that were linked in close proximity through a trifunctional linker to dendritic polyglycerol (dPG). The fluorescence of the donor dye is quenched *via* intramolecular FRET until it is released by cleavage of the acid labile linker to the polymer. This allows one to monitor an increasing fluorescence signal upon dye release in real time, representing the liberation of cargo. We demonstrate the use of this concept in a cell-based microplate assay format, which opens the possibility for high throughput screening approaches (Scheme 1).

Experimental

Reagents

The chemicals used were all commercially available from Aldrich, Acros Organics, Invitrogen, and mivenion GmbH and did not require further purification. All solvents were distilled before usage or purchased dry and in p.a. quality. For preparative work only distilled water and Milli-Q water obtained from a Millipore system were used. Dry solvents were taken from a MB SPS 800 solvent system from MBraun.

Instruments

^{1}H and ^{13}C NMR spectra were recorded on a Jeol ECX-400 (400 MHz ^{1}H-NMR and 176 MHz ^{13}C-NMR) spectrometer or a BrukerBioSpin (700 MHz) instrument at room temperature, and chemical shift values (δ) are given in ppm relative to the internal standard MeOD-d4 ^{1}H-NMR spectra (3.31 ppm), ^{13}C NMR spectra (49.0 ppm). MS ESI-ToF analyses were performed on an Agilent 6210 ESI-TOF, Agilent Technologies, Santa Clara, CA, USA. The fluorescence spectra were recorded on a Jasco FP-6500 spectrofluorometer. UV/Vis spectra were recorded on a Scinco S-3100 spectrometer. The cell-based assay was performed on a Tecan InfiniteM200 Pro microplate reader equipped with a gas control module. For microscopy we used a Leica SP8 confocal laser scanning microscope and LASAF software. The flow cytometric studies were performed with a FACSCanto II flow cytometer (BD Biosciences).

Synthetic procedures

The dPG (average M_W 200 kDa, PDI = 1.6, Fig. S1†) was prepared according to a slightly modified protocol in an emulsion as described earlier.[18] Polyglycerolazide with 1% of the total hydroxyl groups bearing azido groups was prepared as previously described.[19] Briefly, polyglycerolazide was prepared according to a two-step protocol starting from dPG with conversion of the OH groups into mesyl (Ms) groups followed by transformation of the Ms groups into azide (N_3) functionalities (Scheme S1, ESI†). The ICC dyes and IDCC dye (Fig. S2, ESI†) were purchased from mivenion GmbH and synthesized following literature procedures.[20,21] The detailed synthetic procedures of the dye and conjugate synthesis can be found in the ESI.†

Cell viability assay

Cell viability was determined by the CellTiter-Glo® Luminescent Cell Viability Assay (Promega) according to the manufacturer's protocol. After 24 hours of incubation in a serum free medium at a concentration 1 mg mL^{-1} of conjugates, the viability was about 75%.

Fluorescence analysis

The FRET conjugates (10 nM) were incubated in buffers of various pH (4, 5, and 7.4) at 37 °C in a 96-well plate and in a quartz cuvette. A 50 mM phosphate buffer (PB) was used for pH 5 and 7.4 and a 50 mM acetate buffer was used for pH 4. The plate was then placed in the microplate reader. Fluorescence was recorded every 15 minutes at an excitation wavelength of 540 nm (9 nm bandwidth) and an emission wavelength of 580 nm (20 nm bandwidth). Average values from the triplicates were plotted in the graph. Additionally, the fluorescence spectra were recorded after 30 min, 1, 2, 4, 8, and 24 h with a spectrofluorometer to obtain the full fluorescence spectra.

Cell based microplate assay

A549 lung epithelial cancer cells were routinely maintained in DMEM (Life Technologies) with 10% FCS (Biochrom AG, Berlin, Germany) and 1% penicillin/streptomycin (Life Technologies) at 37 °C and 5% CO_2. For the assay, 10 000 cells per well were seeded into 96-well plates and grown overnight. Each 96-well plate contained wells without cells as a control. The next day, cells were washed 3 times with PBS, and 50 μL per well DMEM without FCS and without phenol red was added. For inhibition of cellular uptake, 50 μL of 40 mM methyl-β-cyclodextrin (Sigma) in DMEM was added to the respective wells, giving a final concentration of 20 mM, and incubated

for 15 minutes at 37 °C. After incubation, the respective wells were washed 3 times with 200 μL per well PBS and the compounds were added to final concentrations of 1 mg mL^{-1} in DMEM to the cells, to wells without cells, or in a pH buffer of 4 or 7, each of which was triplicated. Wells, which had been treated with methyl-β-cyclodextrin, were also given Lovastatin (Sigma) with a final concentration of 0.4 μg mL^{-1}. The plates were then placed in the microplate reader, which was equilibrated to 37 °C and 5% CO_2. Fluorescence was recorded every 15 minutes at an excitation wavelength of 540 nm (9 nm bandwidth) and an emission wavelength of 580 nm (20 nm bandwidth). Average values from the triplicates of the control wells without cells were subtracted from the wells with cells and the difference to time point 0 was calculated from the graph. The assay was independently repeated two times to calculate error bars.

Results and discussion

Synthetic strategy for the FRET conjugates

To create an efficient FRET system for monitoring the bond cleavage between a polymeric nanocarrier and a cargo, we followed a modular approach that allowed us to covalently link dPG to two fluorescent dyes in near proximity. Fig. 1 shows the modular design, which comprises dPG as the polymer nanocarrier, lysine attached to the acceptor dye as the trifunctional linker, and the donor dye linked through a pH-sensitive bond.

We chose a commonly known FRET pair of two fluorescent dyes, namely ICC and IDCC. These two dyes showed a suitable degree of spectral overlap between the ICC emission and IDCC absorption spectra, a suitable Förster distance, and sufficient spatial separation of the emission wavelengths for accurate detection.[22] We chose dPG as an example of a nanocarrier because it exhibits good chemical stability, inertness under biological conditions, high biocompatibility, and excellent water solubility. Additionally, dPGs enable selective functionalization of reactive groups, which lead to controllable loadings of bioactive molecules.[23–25] These properties open a broad range of potential applications in medicine and pharmacology, *i.e.* as polymeric nanocarriers, antifouling coatings of biomaterials, targeting moieties, *etc.*[26]

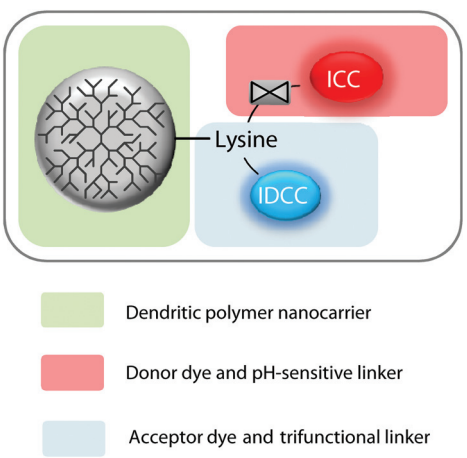

Fig. 1 A modular approach followed for synthesis of the FRET conjugates.

The hydrazone bond was chosen as a pH-sensitive linker to the donor dye ICC due to its proven suitability and adjustable stability against pH-mediated hydrolysis.[6] With such a configuration, it was expected that, upon irradiation of the probe, the fluorescence energy would have been transferred from ICC to IDCC, thereby quenching the ICC fluorescence. Once the acid labile linker cleaved, the ICC should be released, thereby leading to an increase of its fluorescence emission intensity.

The synthetic strategy consists of three consecutive steps: (a) synthesis of the IDCC-labeled tri-functional linker, (b) coupling of the fluorescent linker to the dendritic polymer nanocarrier, and (c) coupling of the pH-sensitive ICC-EMCH linker.

Synthesis of the precursor polymer conjugate

The first step was to prepare the IDCC-labelled polymer precursor with an amino group in near proximity for a later thiolation and thiol–ene click linkage with the EMCH-ICC dyes (Scheme 2). The precursor conjugate was prepared by following procedures previously reported by our group.[27]

Briefly, the fluorenylmethyloxycarbonyl (Fmoc) and *tert*-butyloxycarbonyl (Boc) di-protected amino acid lysine **1** was coupled to propargyl amine through the carboxyl group of the lysine *via* amide bond formation. After Fmoc deprotection the IDCC dye was introduced *via* amide bond formation by an amino-acid coupling strategy. Boc deprotection using trifluoroacetic acid (TFA) gave a free primary amine **3**. The IDCC dye-labelled linker derivatives were purified by reversed phase column chromatography and characterized by ^{1}H-NMR, ^{13}C-NMR, UV-Vis spectroscopy, and MS ESI-ToF. The conjugation of the alkyne and the dye containing linker construct **3** to the polymeric carrier dPG (average M_W 200 kDa) was performed using copper catalyzed Huisgen 1,3-dipolar cycloaddition. The product **4** was purified by ultrafiltration using water as a solvent with one running-cycle with an EDTA solution to remove all the copper content. The conjugate was obtained in 62% yield and characterized by UV-Vis and fluorescence spectroscopy, and fast protein liquid chromatography (FPLC) using a Sephacryl S-100 column.

Synthesis of the pH-sensitive ICC-EMCH linker

For the second synthetic stage we first screened hydrazone-bearing ICC derivatives with optimal pH-stability profiles for

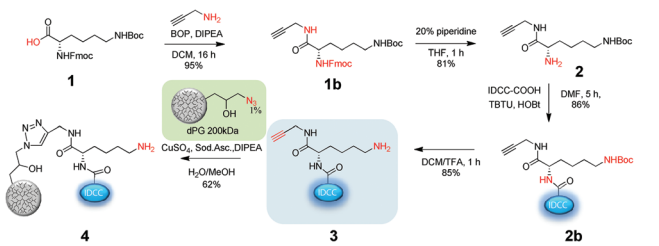

Scheme 2 Synthesis of the IDCC labelled precursor polymer conjugate.

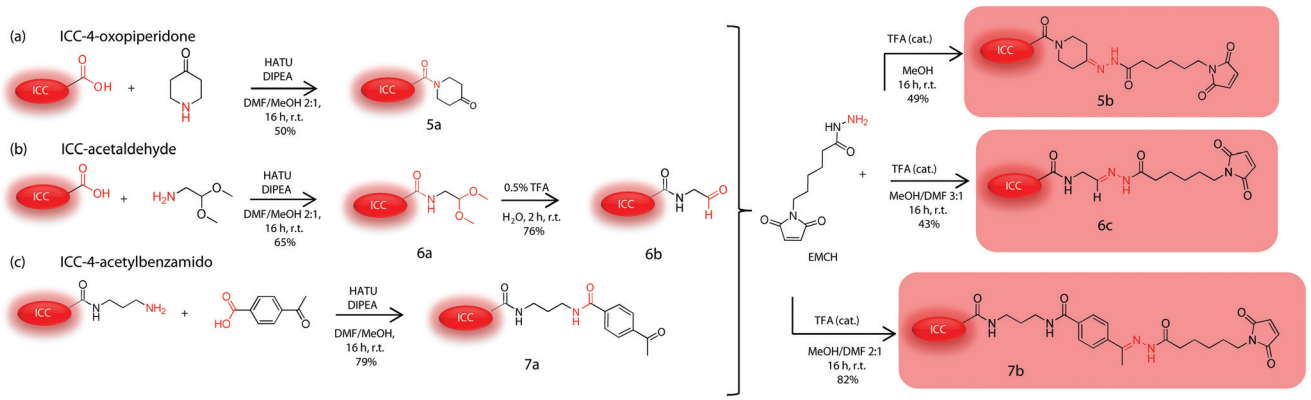

Scheme 3 Synthesis of the hydrazone-bearing derivatives of ICC with different pH-cleavability profiles.

specific intracellular cleavage. The dyes were provided with maleimido groups for the further coupling to the dendritic nanocarrier **4**. Three ICC carbonyl derivatives with different substitutions in the α-position were synthesized (**5a**, **6b**, and **7a** in Scheme 3) as precursors of hydrazone bonds with different stabilities against pH-mediated hydrolysis. (6-Maleimidocaproyl)hydrazine (EMCH) was used as a linker because of its suitable pH-stability profile as earlier reported for other DDS.[3] Therefore, as shown in Scheme 3, two commercially available ICC derivatives were used to form an amide bond with different carbonyl compounds, *i.e.* piperidone, aminoacetaldehyde, and 4-acetylbenzoic acid. The secondary amine of piperidone was used to form an amide bond with ICC carboxylic acid. For this purpose, the coupling reagent *O*-(7-azabenzotriazol-1-yl)-*N*,*N*,*N*′,*N*′-tetramethyluronium hexafluorophosphate (HATU) was applied to form an active ester with the acid *in situ*. Subsequently, piperidone was added to obtain the target product **5a** with a yield of 50%. The synthesis of the second derivative started with the same ICC carboxylic acid but was coupled with the primary amine of aminoacetaldehyde dimethylacetal to yield 65% of the protected aldehyde **6a**. The last variant started with an amino derivative of ICC. The amino group was used to form an amide bond with 4-acetylbenzoic acid to yield 79% of ICC-4-acetylbenzamido **7a** (Scheme 3). In all three cases the carboxylic acid was dissolved together with HATU in a DMF–methanol mixture and DIPEA. This reaction mixture was stirred for 30 minutes to form the active ester. Subsequently the amine compounds were added. After reaction completion the crude products were precipitated in diethyl ether, centrifuged, and the residues were purified using a reversed-phase chromatography column. All compounds were characterized by ^{1}H-NMR and mass spectrometry. The next step was the formation of the hydrazone with the EMCH linker and the different ICC carbonyl derivatives (Scheme 3). The protected aldehyde **6a** was first deprotected under acidic conditions using a catalytic amount of TFA in water. The crude product was purified by reversed phase chromatography. The product **6b** was characterized by ^{1}H-NMR and mass spectrometry. It was obtained with a yield of 76%. The hydrazone synthesis was performed in extra dry methanol and a catalytic amount of TFA. The crude products were purified by reversed-phase chromatography where a quick purification was enforced to avoid the reverse reaction due to water as the eluent. The yield for the ICC-4-oxopiridone-EMCH **5b** was determined to be 49%, for the ICC-acetaldehyde-EMCH **7c** 43%, and the ICC-4-acetylbenzamido derivative **7b** was obtained in 82% yield. Products **5b**, **6c**, and **7b** were characterized by MS ESI-ToF and by ^{1}H-NMR spectroscopy. To quickly assess the stability against hydrolysis in pH 4 and 7.4, a preliminary thin layer chromatography (TLC) study of the three hydrazone derivatives of the ICC dye was performed. It was observed that, as the stability of the hydrazone bond against hydrolysis increased, the rate of dye release decreased. The linker **5b** degraded rapidly at both pH values, rendering this piperidone derivative unsuitable for further investigation. The other two linkers **6c** and **7b** showed sufficient stability at pH 7.4 as expected for linkers used in DDS. The 4-acetylbenzamido derivative **7b** showed higher stability at pH 7.4 and was therefore selected as the ideal building block for the FRET conjugate.

Synthesis of FRET conjugates

In order to synthesize the functional FRET conjugate and a non-cleavable control, the ICC-EMCH linker **7b** or a stable ICC maleimide derivative (ICC-mal, see Fig. S2, ESI†) was conjugated to the precursor polymer conjugate **4** as shown in Scheme 4. Therefore, the free amino group of **4** was thiolated with 2-iminothiolane in (PB) pH 7.4 to yield the conjugate **8**. The resulting thiol was attached either to the maleimido group of the ICC-EMCH **7b** or to the ICC-mal by Michael addition in DMSO. The reaction mixtures were purified using FPLC with a Sephacryl S-100 column and lyophilized. The functional FRET conjugate **9** and the non-cleavable FRET conjugate **10** were characterized by UV/Vis and fluorescence spectroscopy, dynamic light scattering (DLS) and FPLC using a size exclusion gel (Sephacryl S-100) after reconstitution in (PB) (Table 1 and the synthetic part in the ESI†). A CellTiter-Glo® assay demonstrated that neither the precursor polymer conjugate nor the conjugation of the ICC dye significantly influenced the cell viability (Fig. S3†).

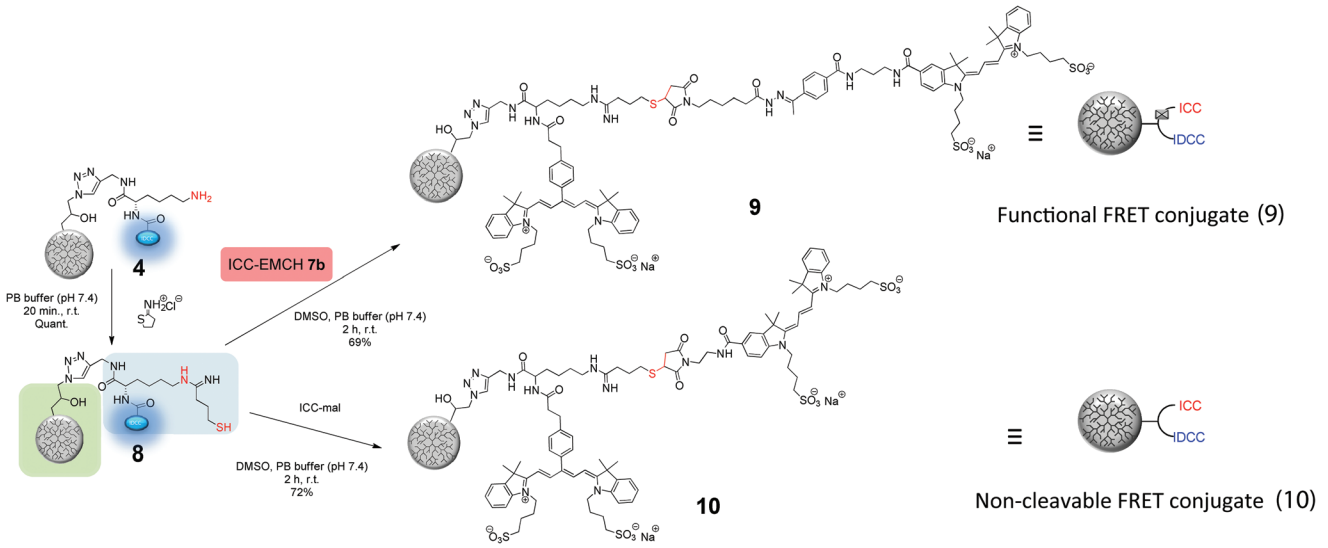

Scheme 4 Synthesis of the FRET conjugates starting from the precursor conjugate **4**. Two consecutive conjugation reactions yield either the functional (**9**) or the non-cleavable FRET conjugate **10**.

Table 1 Physico-chemical parameters of the conjugates

Compound	Dye loading [w%] (IDCC/ICC)[a]	Dye molar ratio (IDCC/ICC)[a]	M_w [b] [kDa]	M_w/M_n	d [c] [nm]
Conjugate **9**	0.29/0.11	1/0.4	200	1.6	12.5
Conjugate **10**	0.24/0.12	1/0.5	200	1.6	12.1

[a] Determined by UV/Vis-spectrometry using the absorption coefficient of the IDCC dye. [b] The average value determined by GPC. [c] The mean hydrodynamic diameter as obtained by the size distribution by volume *via* DLS measurements in PBS (pH 7.4).

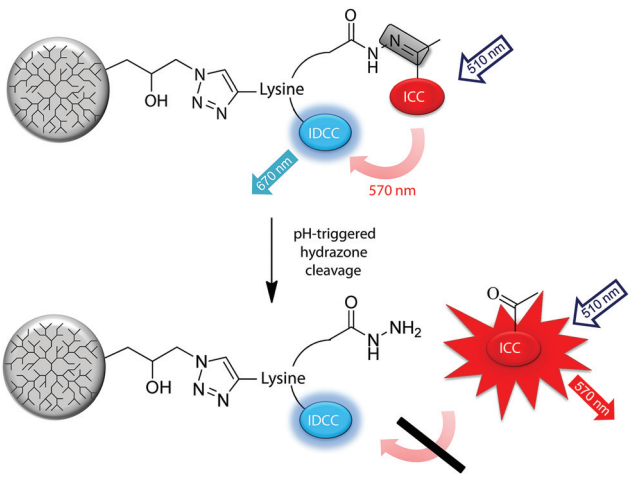

Fig. 2 Schematic illustration of the intramolecular FRET between ICC and IDCC being disrupted upon pH mediated cleavage.

Evaluation of the FRET conjugates

In order to prove the feasibility of our system to monitor the intracellular cleavage and dye release, the FRET conjugate was incubated in buffer solutions at different biologically relevant pH values (4, 5, and 7.4) and the fluorescence intensity was measured over time. As discussed above and depicted in Fig. 2, the fluorescence intensity of the donor dye ICC should increase over time upon pH-mediated cleavage of the hydrazone linker.

The fluorescence spectra of the conjugate **9** that was incubated at pH 4 over time are shown in Fig. 3a. It shows a strong increase in donor dye fluorescence at 568 nm and a reduction of the acceptor induced peak at 667 nm over time. To confirm that the increase of fluorescence was due to the pH mediated cleavage of the hydrazone bond, the non-cleavable control **10** was investigated. As expected, the fluorescence spectra of **10** did not show any change in the intensity over time (Fig. 3b). Fig. 3c and 3d summarize the fluorescence measurements of the two conjugates at different relevant pH values (4, 5, and 7.4). The normalized fluorescence intensity was plotted against the time of incubation in the respective buffer solution. It was observed that the fluorescence of the FRET-probe and the corresponding control suffered only marginal changes at pH 7.4, whereas the fluorescence of the functional FRET conjugate **9** at pH 5 increased to a lesser extent when compared to the results at pH 4. The quenching efficiency of the FRET conjugate **9** was calculated to be 75% using eqn (S1) (ESI†).

We demonstrate that our approach allows facile coupling of the functional FRET moiety to a polymer containing a low amount of azides, as well as the incorporation of a linker with enough stability against hydrolysis. To a large extent this strategy would allow the incorporation of different linker modalities, *e.g.* enzymatic or reductive cleavable linkers, to cover a greater area of triggered release applications.

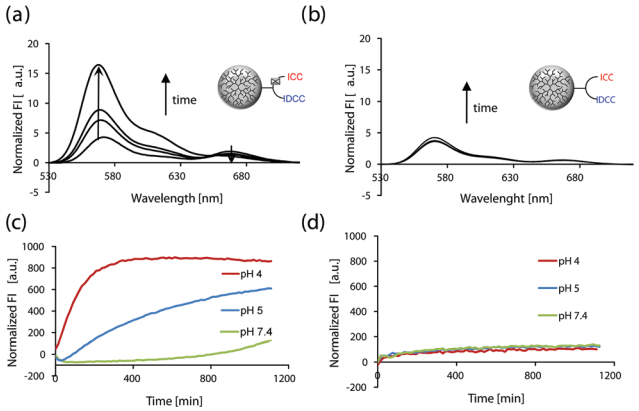

Fig. 3 Fluorescence analysis of the conjugates. (a, b) Fluorescence spectra of the functional conjugate **9** and the non-cleavable control **10** incubated at pH 4, excited at 500 nm, over time. (c, d) The fluorescence intensity of the two conjugates (**9** and **10**, respectively) plotted over time with incubation at different relevant pH values (4, 5, and 7.4) in a microplate reader.

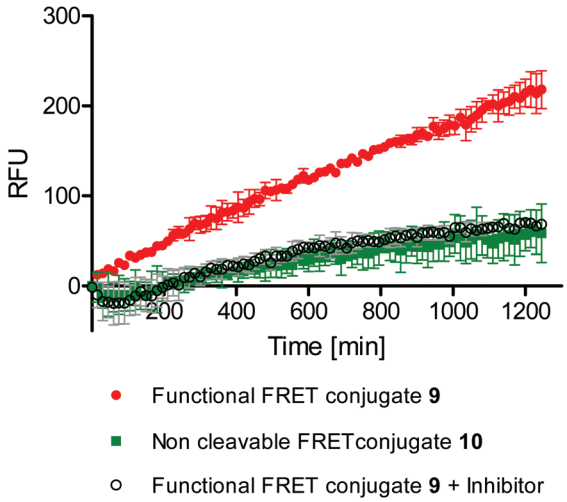

Fig. 4 Change in the fluorescence intensities (in relative fluorescence units [RFU]) over time of the different conjugates in a cell-based microplate assay.

Utilization of the probe to monitor intracellular cargo release

According to our hypothesis the synthesized probes should enable monitoring events like bond cleavage and cargo release within acidic compartments of living cells. Moreover, we thought that the probes could be applied in a high throughput screening compatible microplate assay. To this end, A549 cancer cells were incubated with the FRET conjugate **9** on 96-well plates and grown inside a microplate reader which recorded the fluorescence intensity of the ICC dye over time. As a control for media effects, which could possibly occur independently of the cells, the same plate contained control wells without cells but only the conjugates in cell culture media. The fluorescence intensity values of these control wells were subtracted from those of the wells containing cells. Values were then calculated and expressed as a change relative to the starting time point. A plot of the relative fluorescence intensities over time with the background subtracted is shown in Fig. 4. Fluorescence intensity of the ICC dye of the functional conjugate steadily increased over time (Fig. 4, red line). To confirm that this increase was due to pH mediated cleavage of the hydrazone bond and thereby release of the ICC dye, we included the non-cleavable conjugate **10** on the same 96-well plate under identical conditions. This non-cleavable control conjugate showed only a marginal increase of fluorescence intensity over time (Fig. 4, green line). This result confirmed that the regained fluorescence signal was due to the cleavage of the ICC dye. To further prove that the bond was cleaved within the cells after uptake, the 96-well plate also included cells that had been pre-treated with endocytosis inhibitors (Fig. 4, grey line). In this case the fluorescence intensity only marginally increased, similar to the non-cleavable control.

Successful uptake and inhibition were confirmed by confocal microscopy and by flow cytometric studies (Fig. S4–S6, ESI†). Due to the fact that the released ICC is not accumulating intracellularly it could not be imaged with these methods. Nevertheless, the results from the microplate reader highlight the superior performance of the assay that enables monitoring the sum of all cleavage events from 10 000 cells per well.

Altogether, these results confirmed that the increased fluorescence seen in the turn-on probe **9**, which was incubated on and monitored over time in living cells, was due to an acidic bond cleavage after cellular uptake. Therefore we have demonstrated the application of our probe in a cell-based, real time, and high throughput compatible microplate assay, which can provide valuable insight into the event of bond cleavage in cells and thus help to evaluate the performance of a polymeric nanocarrier.

Conclusions

The comparison of DDS in terms of their efficiency is of great importance to estimate whether novel nanocarriers are worth future research. In the particular case of polymer–drug conjugates, information about intracellular linker cleavage and release kinetics is crucial for the quick assessment of their suitability.

In this paper, we have developed a turn-on probe which utilizes the FRET phenomenon of the dyes ICC and IDCC attached to a polymeric carrier to monitor the cleavage of a linker and consequent release of a cargo. This functional polymeric probe was synthesized using a tri-functional alkyne and IDCC containing linker and a pH labile, conjugatable (maleimide bearing) ICC derivative. When the conjugate was cleaved, the attached ICC dye was released and its fluorescence, which had been quenched before, increased.

We suggest the use of this assay as a platform technology for testing the performance of polymer–drug conjugates. For this purpose, we showed that the probe could be applied in a cell-based microplate assay that allowed real time monitoring

and high throughput approaches. It induced a signal when the conjugate uptake occurred and the cargo was released. This probe design can easily be applied to other polymers containing azide groups by attachment of the alkyne and IDCC containing linker **3** and subsequent conjugation of the ICC-EMCH derivative. Furthermore, both the cleavage modality and the cell line can be varied, depending on the purpose of the polymer conjugate which is investigated. This would enable the rapid determination of structure–activity relationships of various nanocarriers.

Acknowledgements

The authors would like to thank the financial support from the Bundesministerium für Bildung und Forschung (BMBF) through the ThermoNanogele NanoMatFutur award (13N12561) and the Freie Universität Focus Area Nanoscale. We gratefully acknowledge Dr Pamela Winchester for proofreading the manuscript.

Notes and references

1 R. A. Petros and J. M. DeSimone, *Nat. Rev. Drug Discovery*, 2010, **9**, 615–627.
2 R. Duncan, *Nat. Rev. Drug Discovery*, 2003, **2**, 347–360.
3 R. Haag and F. Kratz, *Angew. Chem., Int. Ed.*, 2006, **45**, 1198–1215.
4 R. K. Jain, *Cancer Res.*, 1987, **47**, 3039–3051.
5 Y. Matsumura and H. Maeda, *Cancer Res.*, 1986, **46**, 6387–6392.
6 M. Calderón, M. A. Quadir, M. Strumia and R. Haag, *Biochimie*, 2010, **92**, 1242–1251.
7 J. Yang, H. Chen, I. R. Vlahov, J.-X. Cheng and P. S. Low, *Proc. Natl. Acad. Sci. U. S. A.*, 2006, **103**, 13872–13877.
8 S. Buckhout-White, J. C. Claussen, J. S. Melinger, Z. Dunningham, M. G. Ancona, E. R. Goldman and I. L. Medintz, *RSC Adv.*, 2014, **4**, 48860–48871.
9 W.-H. Chen, G.-F. Luo, X.-D. Xu, H.-Z. Jia, Q. Lei, K. Han and X.-Z. Zhang, *Nanoscale*, 2014, **6**, 9531–9535.
10 H.-Y. Hu, D. Vats, M. Vizovisek, L. Kramer, C. Germanier, K. U. Wendt, M. Rudin, B. Turk, O. Plettenburg and C. Schultz, *Angew. Chem., Int. Ed.*, 2014, **53**, 7669–7673.
11 G. O. Menéndez, C. S. López, E. A. Jares-Erijman and C. C. Spagnuolo, *Photochem. Photobiol.*, 2013, **89**, 1354–1361.
12 A. M. Hessels and M. Merkx, *Metallomics*, 2014, DOI: 10.1039/c4mt00179f.
13 J. Yang, H. Chen, I. R. Vlahov, J.-X. Cheng and P. S. Low, *J. Pharmacol. Exp. Ther.*, 2007, **321**, 462–468.
14 Y. Li, T.-y. Lin, Y. Luo, Q. Liu, W. Xiao, W. Guo, D. Lac, H. Zhang, C. Feng, S. Wachsmann-Hogiu, J. H. Walton, S. R. Cherry, D. J. Rowland, D. Kukis, C. Pan and K. S. Lam, *Nat. Commun.*, 2014, 5.
15 Y. Li, W. Xiao, K. Xiao, L. Berti, J. Luo, H. P. Tseng, G. Fung and K. S. Lam, *Angew. Chem., Int. Ed.*, 2012, **51**, 2864–2869.
16 F. Wang, Y.-C. Wang, S. Dou, M.-H. Xiong, T.-M. Sun and J. Wang, *ACS Nano*, 2011, **5**, 3679–3692.
17 J. Wang, P. P. Gao, X. X. Yang, T. T. Wang, J. Wang and C. Z. Huang, *J. Mater. Chem. B*, 2014, **2**, 4379–4386.
18 R. K. Kainthan, E. B. Muliawan, S. G. Hatzikiriakos and D. E. Brooks, *Macromolecules*, 2006, **39**, 7708–7717.
19 S. Roller, H. Zhou and R. Haag, *Mol. Diversity*, 2005, **9**, 305–316.
20 J. Pauli, K. Licha, J. Berkemeyer, M. Grabolle, M. Spieles, N. Wegner, P. Welker and U. Resch-Genger, *Bioconjugate Chem.*, 2013, **24**, 1174–1185.
21 K. Licha, C. Hessenius, A. Becker, P. Henklein, M. Bauer, S. Wisniewski, B. Wiedenmann and W. Semmler, *Bioconjugate Chem.*, 2001, **12**, 44–50.
22 A. Iqbal, S. Arslan, B. Okumus, T. J. Wilson, G. Giraud, D. G. Norman, T. Ha and D. M. J. Lilley, *Proc. Natl. Acad. Sci. U. S. A.*, 2008, **105**, 11176–11181.
23 M. Calderón, P. Welker, K. Licha, I. Fichtner, R. Graeser, R. Haag and F. Kratz, *J. Controlled Release*, 2011, **151**, 295–301.
24 A. F. Hussain, H. R. Krüger, F. Kampmeier, T. Weissbach, K. Licha, F. Kratz, R. Haag, M. Calderón and S. Barth, *Biomacromolecules*, 2013, **14**, 2510–2520.
25 M. Calderón, S. Reichert, P. Welker, K. Licha, F. Kratz and R. Haag, *J. Biomed. Nanotechnol.*, 2014, **10**, 92–99.
26 M. Calderón, M. A. Quadir, S. K. Sharma and R. Haag, *Adv. Mater.*, 2010, **22**, 190–218.
27 H. R. Krüger, I. Schütz, A. Justies, K. Licha, P. Welker, V. Haucke and M. Calderón, *J. Controlled Release*, 2014, **194**, 189–196.

